**NONLINEAR ANALYSIS
OF A CLASS B FREQUENCY DOUBLER**

OSA-94-OS-4-R

March 23, 1994

Optimization Systems Associates Inc.

Introduction

A class B frequency doubler is the second CAD benchmark example provided by *Microwave Engineering Europe* for large-signal simulation. The problem statement was received by fax from the Editor on February 24 and on March 1, 1994. It was augmented by a missing data item on March 7, with another data item corrected on March 23. We used HarPE [1], OSA90/hope [2] and Sonnet's *em* [3] to carry out modeling of the NE71000 FET and nonlinear analysis of the doubler.

A. FET Parameter Extraction

Since no large-signal model of the FET was provided by the editor, nor it was available from the manufacturer, we used HarPE to perform parameter extraction to create the large-signal FET model. The data that we utilized for parameter extraction contain typical DC characteristics and typical S parameters from 2 GHz to 26 GHz with 1 GHz step at two bias points published in the "NEC California Eastern Laboratories, RF and microwave Semiconductors" data book [4]. The built-in Curtice and Ettenberg model together with the Extrinsic4 linear subcircuit is chosen to model the FET. The parameter extraction is performed by fitting simultaneously the DC curves at 12 points, and the S parameters at the two bias points and 25 frequencies. Very good DC match and reasonable S-parameter match are obtained.

B. Nonlinear Harmonic Balance simulation

We use OSA90/hope to carry out the nonlinear harmonic balance (HB) simulation of the overall circuit with various component simulations, as summarized by the following three cases.

Case I: All microstrip components are simulated using OSA90/hope's built-in models. This naturally does not include couplings between the components.

Case II: The third harmonic stubs situated at the gate and drain ports of the FET are simulated by *em* [3]. This reflects the coupling between the two stubs.

Case III: In addition to the third harmonic stubs, the bias pads together with the radial stubs are also simulated by *em* [3]. This reflects the couplings in the biasing subcircuit as well as between the third harmonic stubs.

The conversion gain is calculated by

conversion gain = output power at the second harmonic / available input power.

Results for Case I:

In this case we simulate the circuit by considering all the microstrip elements as independent elements. We use OSA90/hope's built-in microstrip empirical models for all transmission lines, stubs, pads and discontinuities. This approach neglects any couplings between the components, in particular the third harmonic stubs situated at the gate and drain ports of the FET and the bias pads.

The output power and conversion gain versus input power at 7 GHz are shown in Figs. 1 and 2, respectively. The output power and conversion gain versus frequency at 9 dBm input power are shown in Figs. 3 and 4, respectively. A 3D view of conversion gain versus frequency and input power is given in Fig. 5. The source and output voltage waveforms at 7 GHz and 9 dBm input power are plotted in Fig. 6.
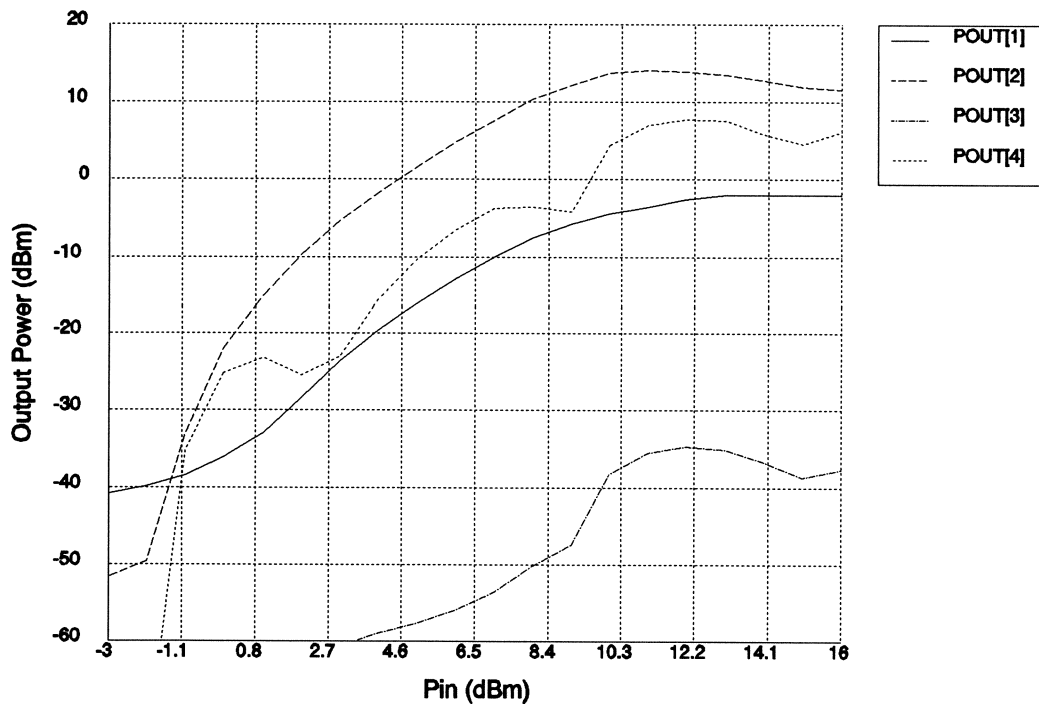

Fig. 1 Output power versus input power at 7 GHz. Couplings are not taken into account.
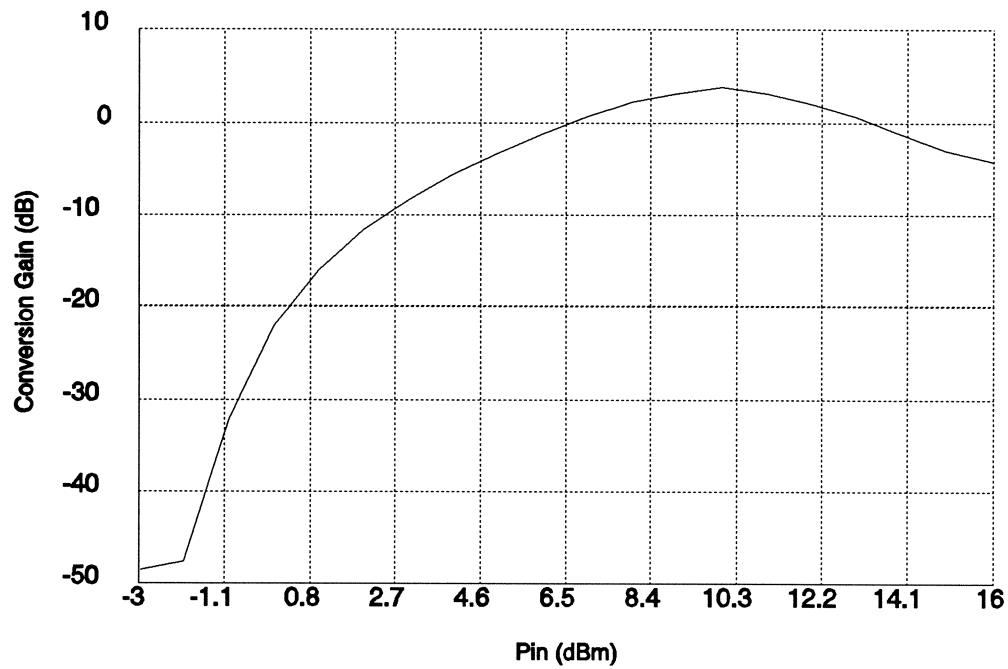
Fig. 2 Conversion gain versus input power at 7 GHz. Couplings are not taken into account.
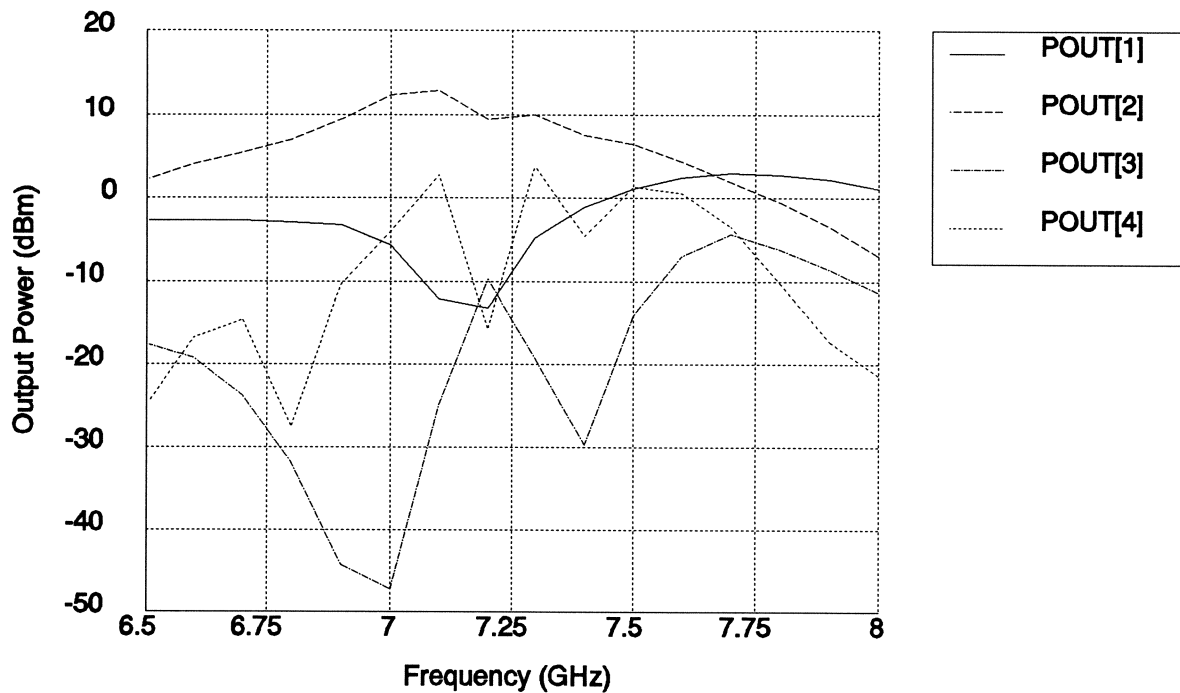

Fig. 3 Output power versus frequency at 9 dBm input power. Couplings are not taken into account.
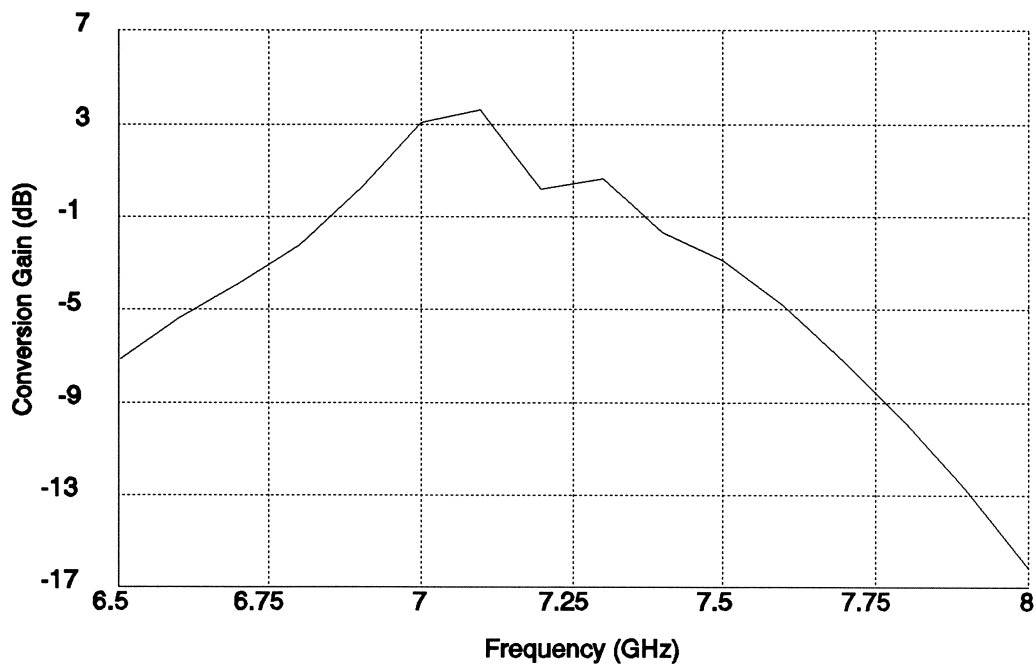
Fig. 4 Conversion gain versus frequency at 9 dBm input power. Couplings are not taken into account.
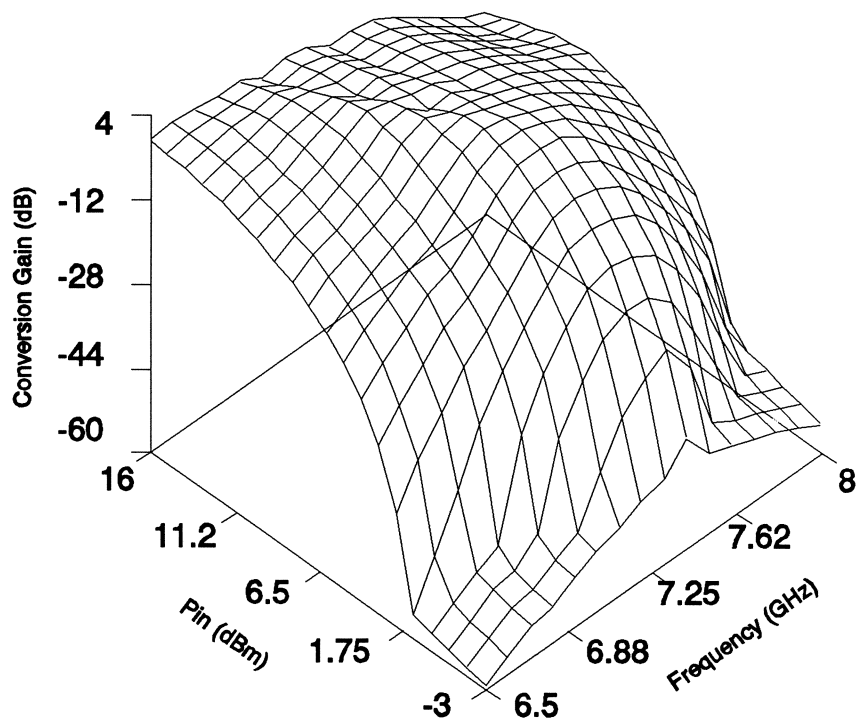

Fig. 5 3D view of conversion gain versus input power and frequency. Couplings are not taken into account.
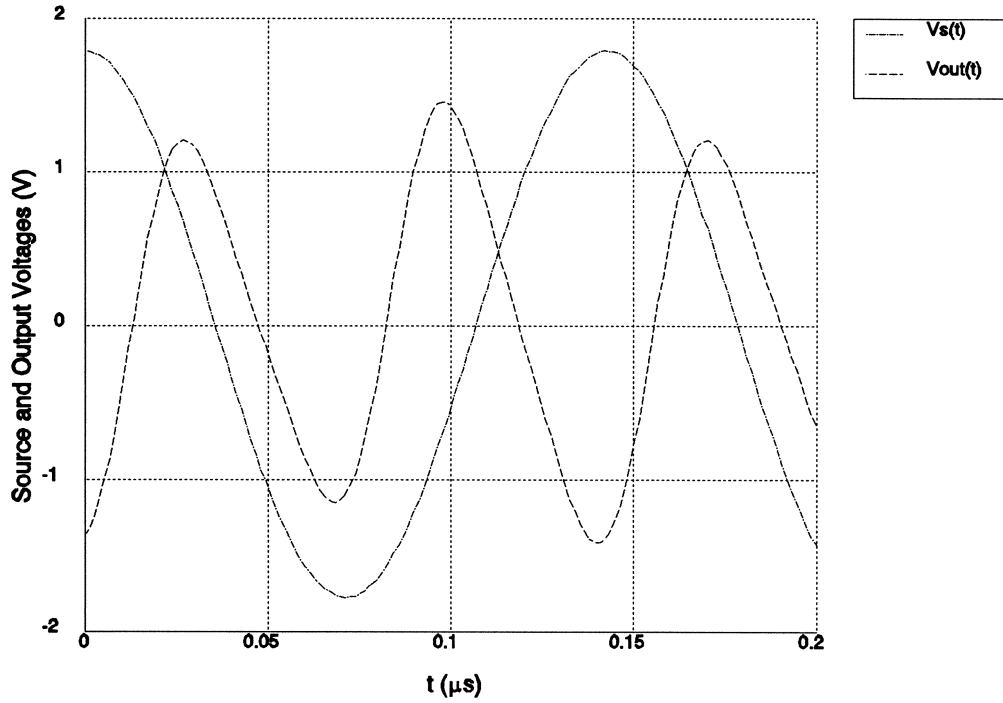
Optimization Systems Associates Inc.

Fig. 6   Source and output voltage waveforms at 7 GHz and 9 dBm input power. Couplings are not taken into account.

Results for Case II:

In this case we consider the coupling effect of the third harmonic stubs situated at the gate and drain ports of the FET. Both stubs are considered as one four-port element which is simulated by *em* [3] and imported to OSA90/hope for circuit-level simulation.

The output power and conversion gain versus input power at 7 GHz are shown in Figs. 7 and 8, respectively. The output power and conversion gain versus frequency at 9 dBm input power are shown in Figs. 9 and 10, respectively. A 3D view of conversion gain versus frequency and input power is given in Fig. 11. The source and output voltage waveforms at 7 GHz and 9 dBm input power are plotted in Fig. 12.
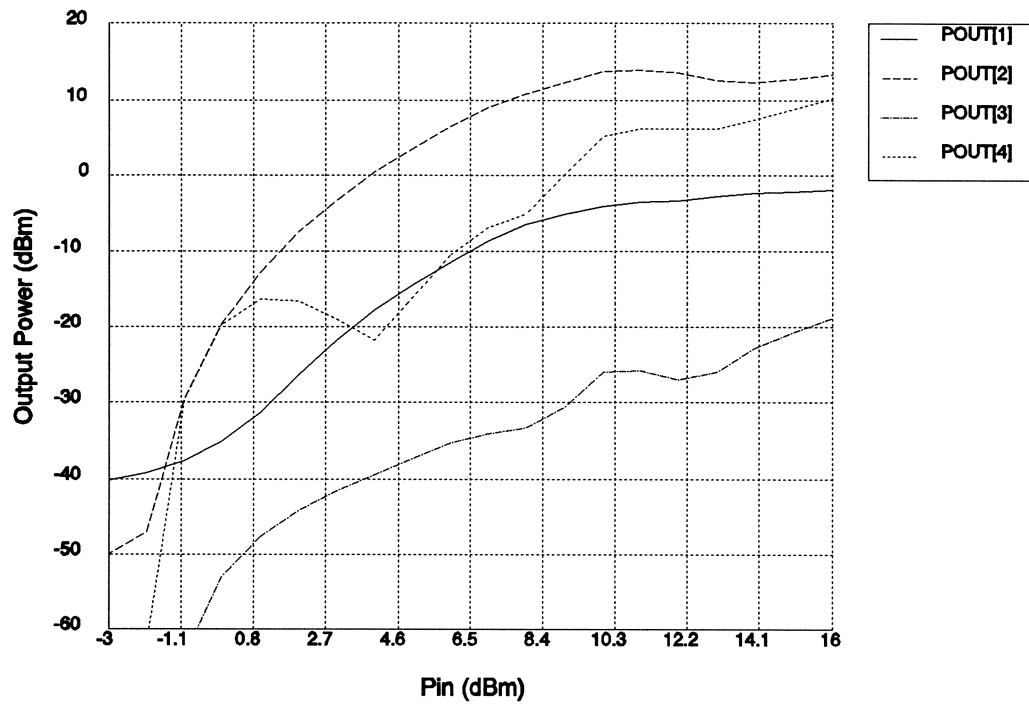
Fig. 7 Output power versus input power at 7 GHz. The coupling between the third harmonic stubs is simulated by *em* [3].
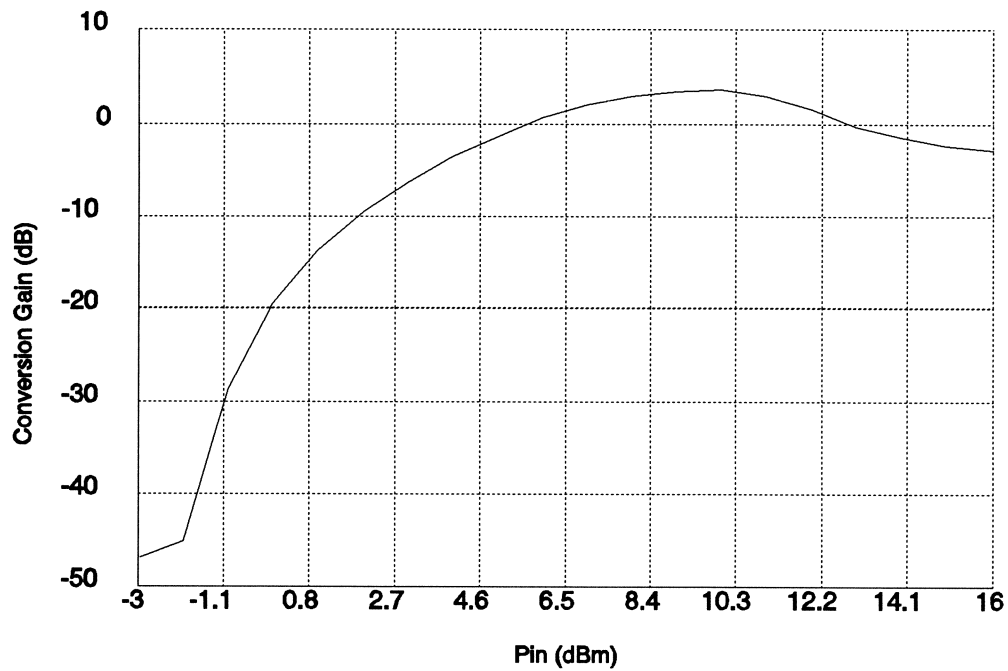

Fig. 8 Conversion gain versus input power at 7 GHz. The coupling between the third harmonic stubs is simulated by *em* [3].

6

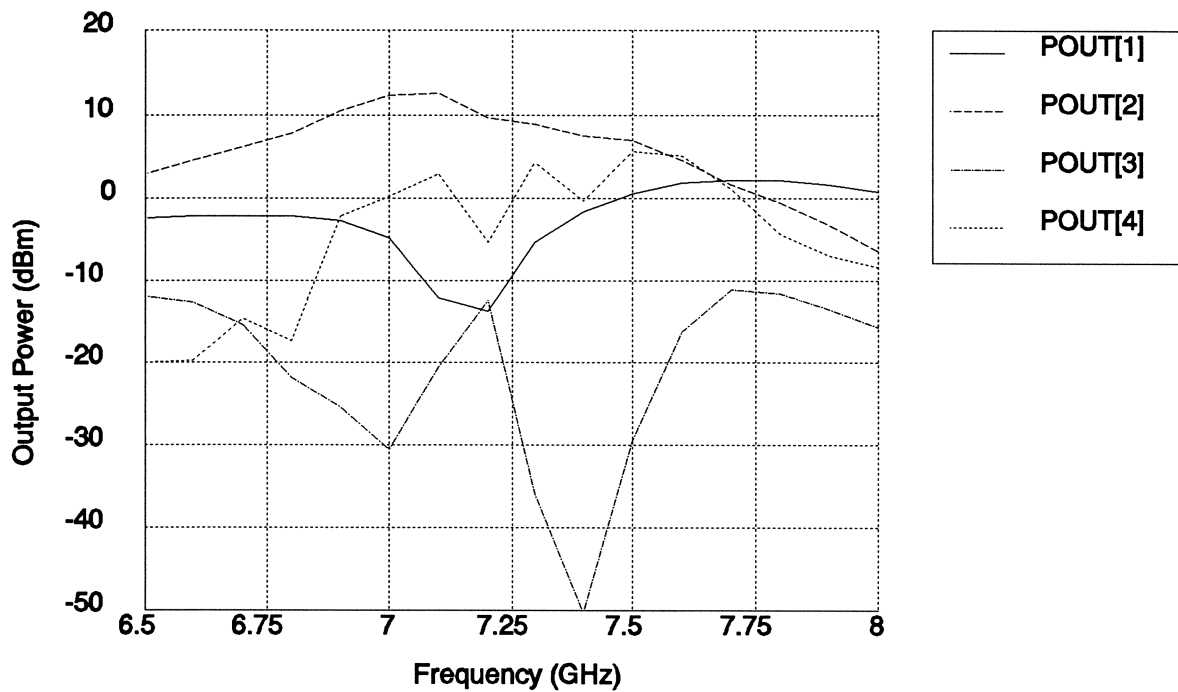*Optimization Systems Associates Inc.*

Fig. 9 Output power versus frequency at 9 dBm input power. The coupling between the third harmonic stubs is simulated by *em* [3].
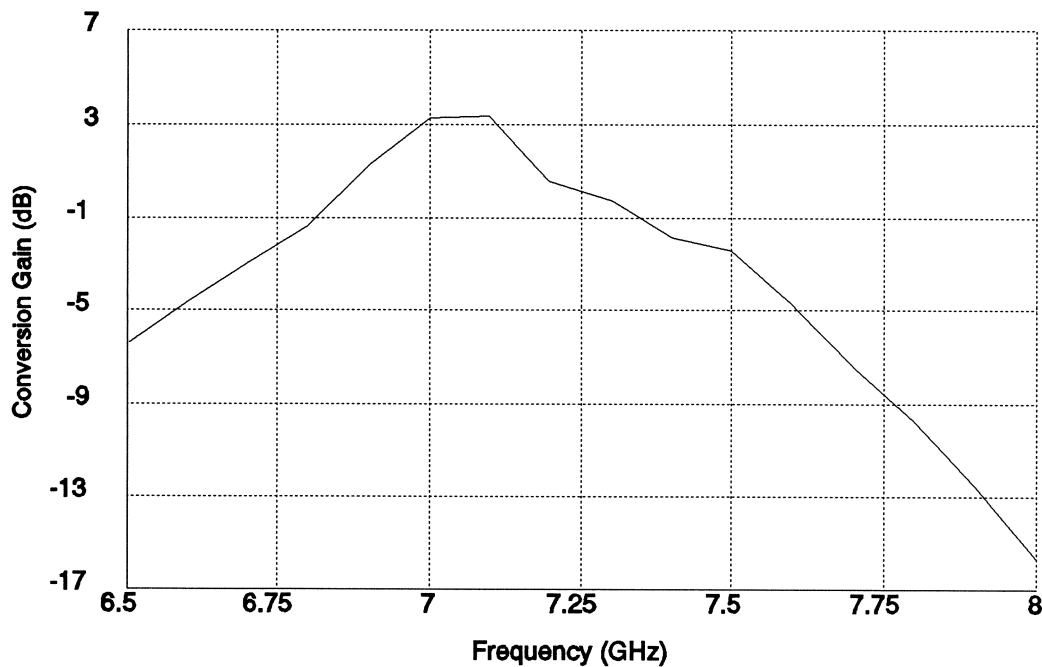
Fig. 10 Conversion gain versus frequency at 9 dBm input power. The coupling between the third harmonic stubs is simulated by *em* [3].
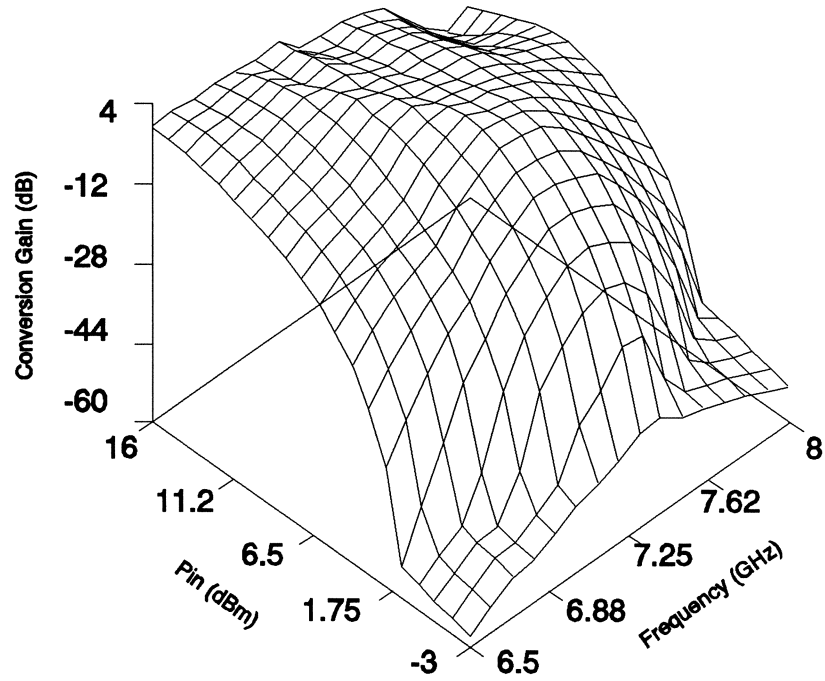
7

Fig. 11   3D view of conversion gain versus input power and frequency. The coupling between the
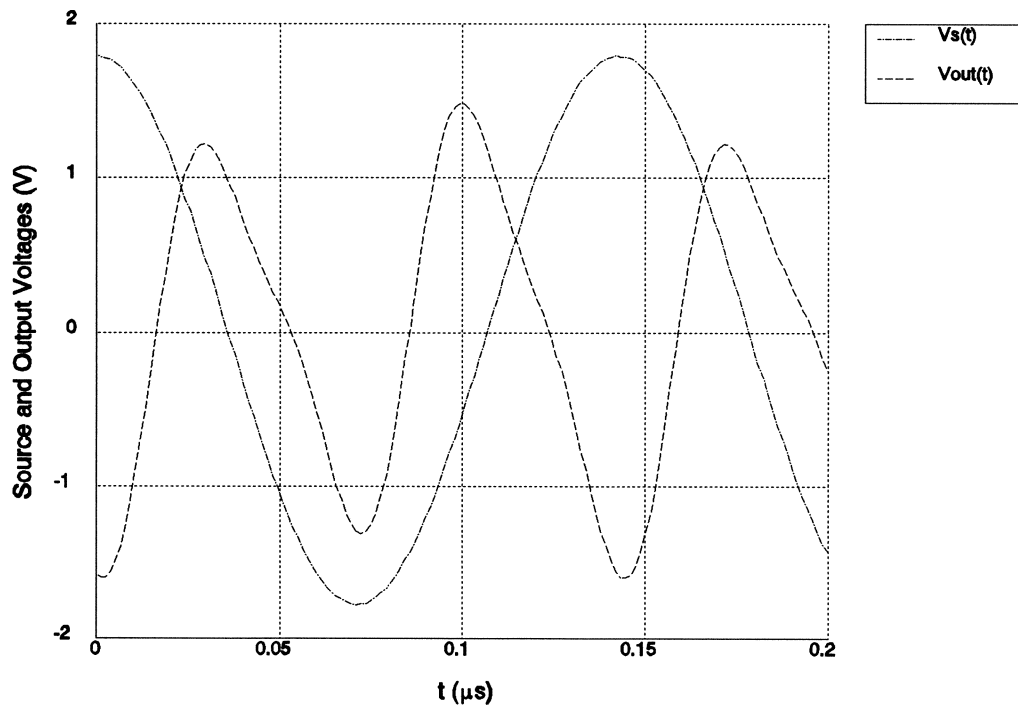third harmonic stubs is simulated by *em* [3].

Fig. 12   Source and output voltage waveforms at 7 GHz and 9 dBm input power. The coupling
between the third harmonic stubs is simulated by *em* [3].

Comparing Fig. 7 with Fig. 4 we can see that the output power at the third and fourth harmonics at 7 GHz of Case II are higher than those of Case I. Due to the coupling effect the resulting output waveform is slightly more distorted, as seen by comparing Figs. 6 and 12.

Results for Case III:

In this case we consider both the coupling of the third harmonic stubs situated at the gate and drain ports of the FET and the effect of the bias pads. In addition to the third harmonic stubs, each bias pad together with the adjacent radial stub is also simulated by *em* [3] as a two-port. These three subcircuits are simulated by *em* [3] and imported into OSA90/hope for overall circuit-level simulation. This reflects the couplings within those three subcircuits (the third harmonic stubs, the gate biasing circuit, and the drain biasing circuit).

The output power and conversion gain versus input power at 7 GHz are shown in Figs. 13 and 14, respectively. The output power and conversion gain versus frequency at 9 dBm input power are shown in Figs. 15 and 16, respectively. A 3D view of conversion gain versus frequency and input power is given in Fig. 17. The source and output voltage waveforms at 7 GHz and 9 dBm input power are plotted in Fig. 18.

Comparing the results of this case with those of Case I and Case II, we can see that the effect of couplings between the bias pads and the radial stubs is quite significant. The output waveform is significantly distorted as seen from Fig. 18.

Fig. 13   Output power versus input power at 7 GHz. The couplings between the third harmonic stubs and between the bias pads and the corresponding radial stubs are simulated by *em* [3].
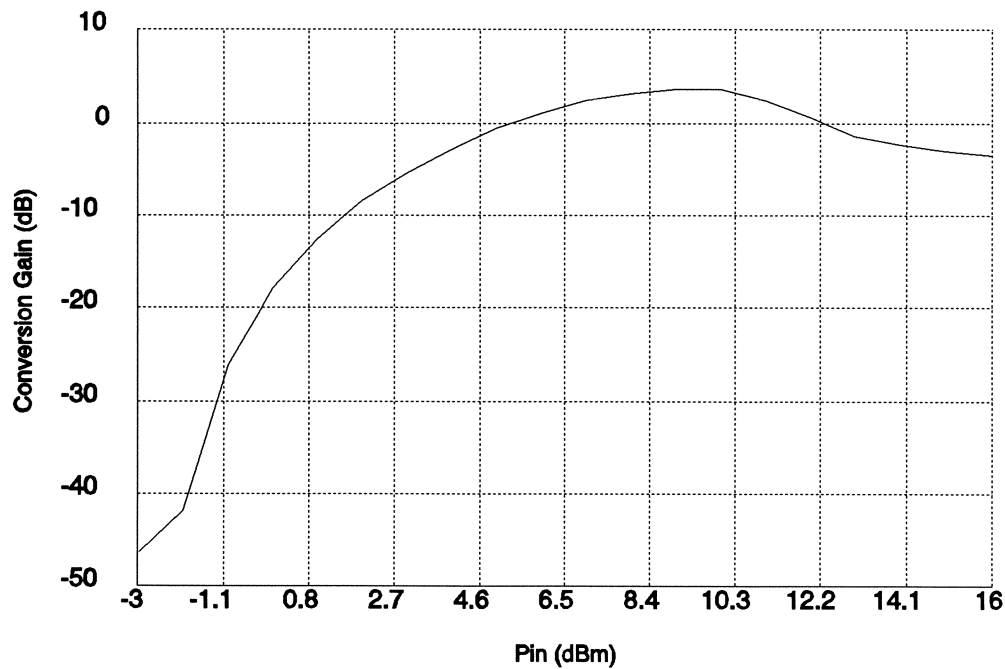
Fig. 14   Conversion gain versus input power at 7 GHz. The couplings between the third harmonic stubs and between the bias pads and the corresponding radial stubs are simulated by *em* [3].
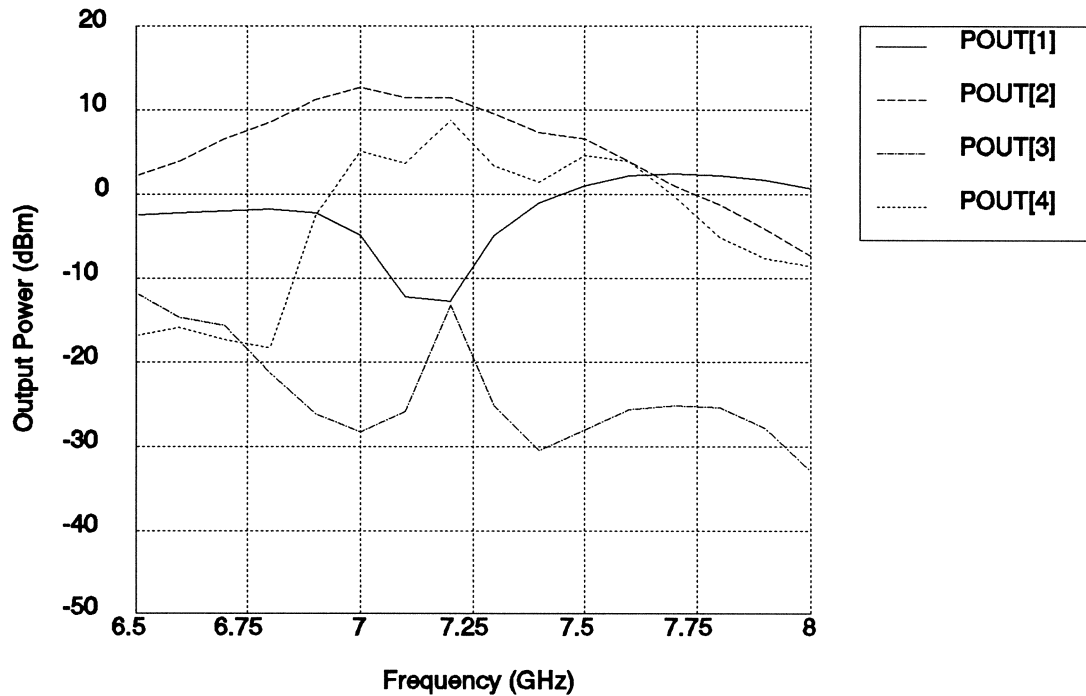
Fig. 15 Output power versus frequency at 9 dBm input power. The couplings between the third harmonic stubs and between the bias pads and the corresponding radial stubs are simulated by *em* [3].
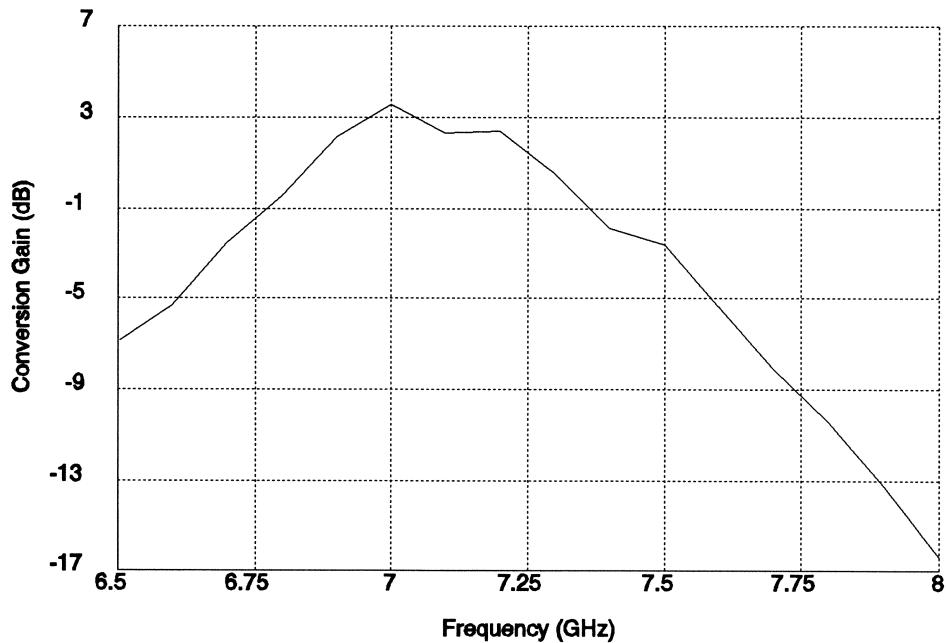
Fig. 16 Conversion gain versus frequency at 9 dBm input power. The couplings between the third harmonic stubs and between the bias pads and the corresponding radial stubs are simulated by *em* [3].
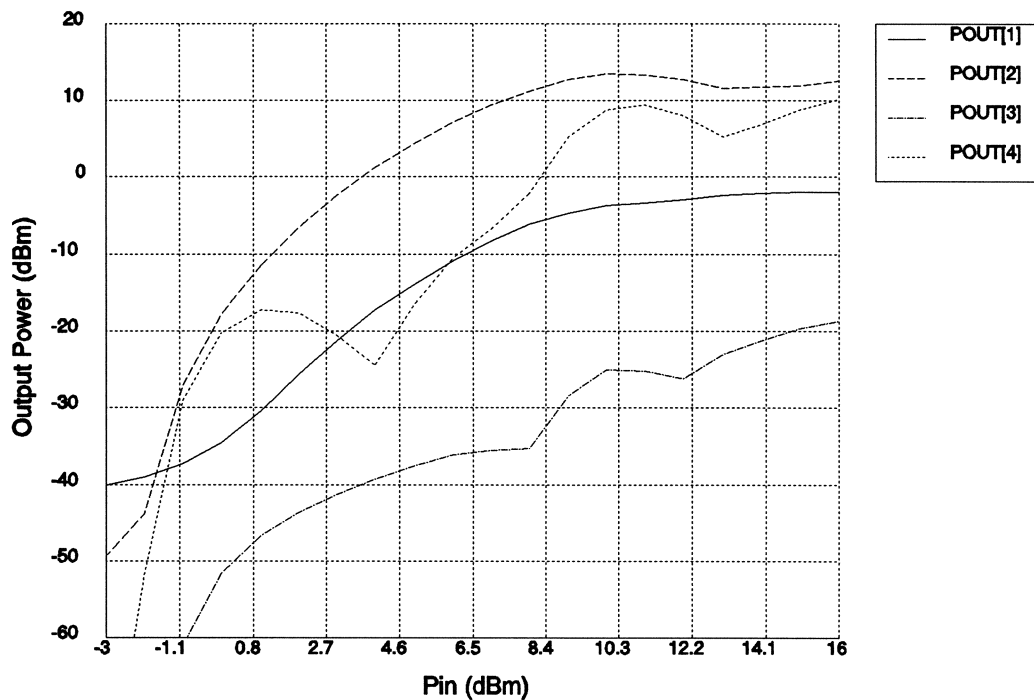
11

Fig. 17 3D view of conversion gain versus input power and frequency. The couplings between the third harmonic stubs and between the bias pads and the corresponding radial stubs are simulated by *em* [3].
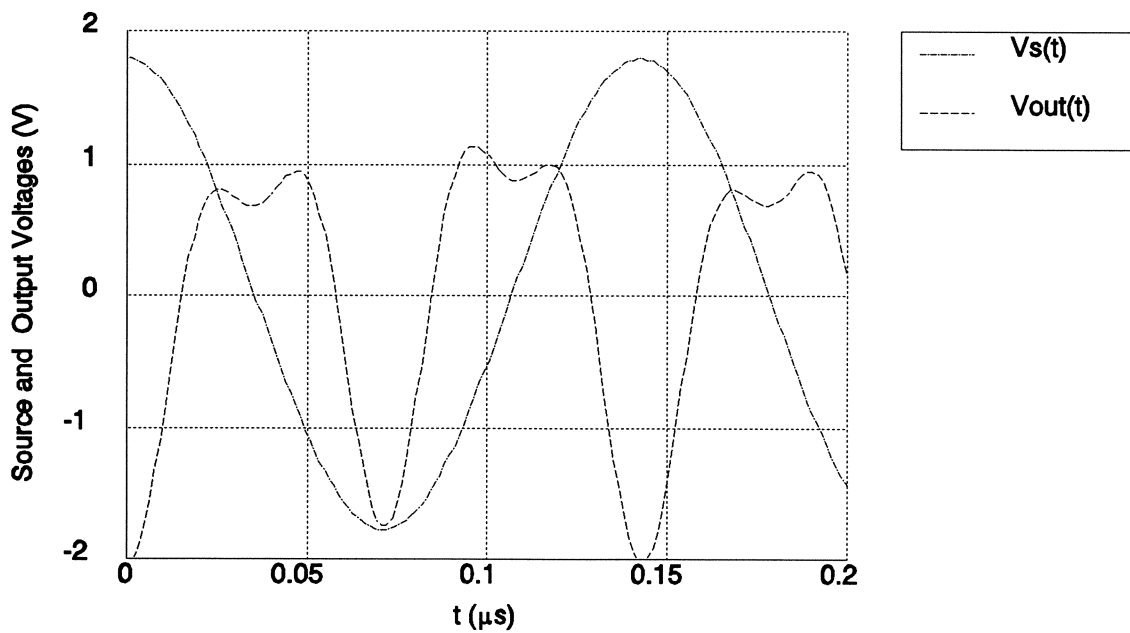
Fig. 18 Input and output voltage waveforms at 7 GHz and 9 dBm input power. The couplings between the third harmonic stubs and between the bias pads and the corresponding radial stubs are simulated by *em* [3].
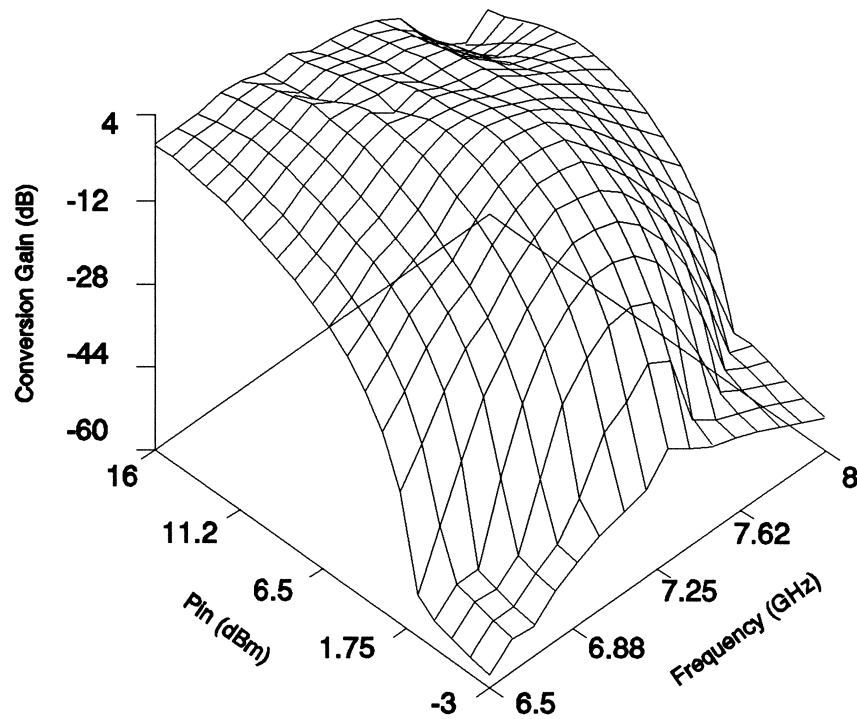
C. Statistical Analysis

To investigate the effect of the FET model uncertainty on the simulation result of the circuit, we perform statistical Monte Carlo analysis by assigning tolerances to the model parameters. A uniform distribution with 20 % tolerance is assigned to all model parameters. Monte Carlo analysis with OSA90/hope's built-in microstrip component models (as in Case I) is carried out using 50 outcomes.

The Monte Carlo sweep of the conversion gain versus input power at 7 GHz is shown in Fig. 19. The conversion gain at 7 GHz and 9 dBm input power are spread between -2.4 dB and 4.7 dB. This reflects the model uncertainty and is illustrated by the histogram shown in Fig. 20. 20 % tolerance is quite large, particularly when the parameters are statistically independent. This means that this estimate of the gain spread is fairly pessimistic. In other words, the effect of doubling the frequency is not very sensitive to the transistor parameters, though the spectral purity of the output waveform may be.
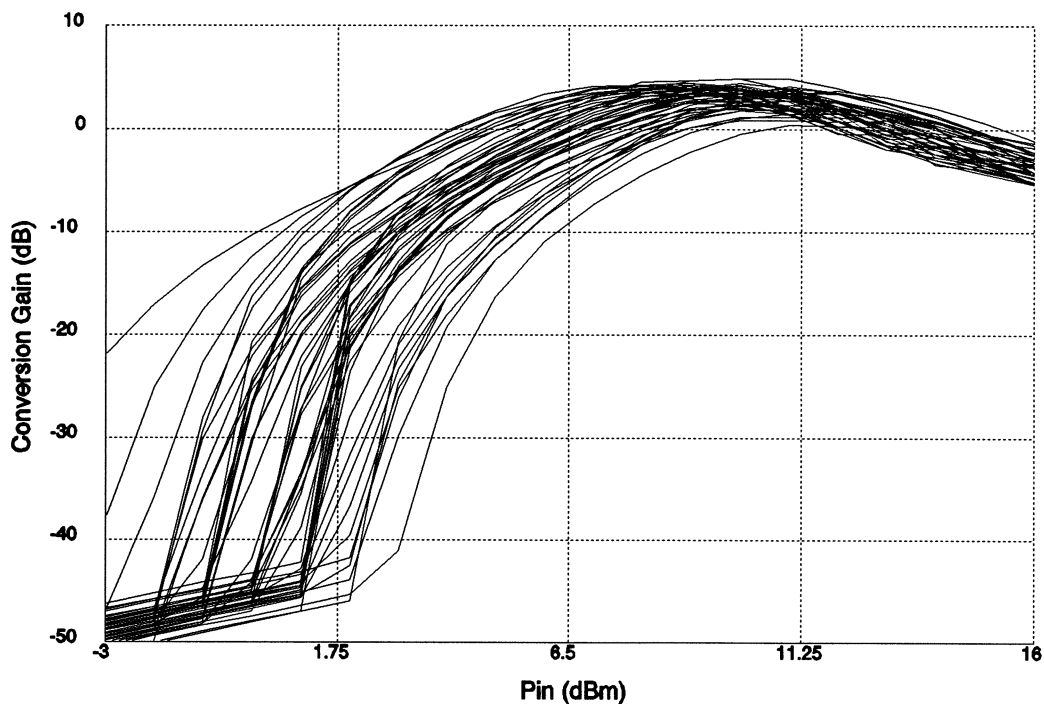
Fig. 19   Monte Carlo sweep of conversion gain versus input power at 7 GHz. Couplings are not taken into account.

13
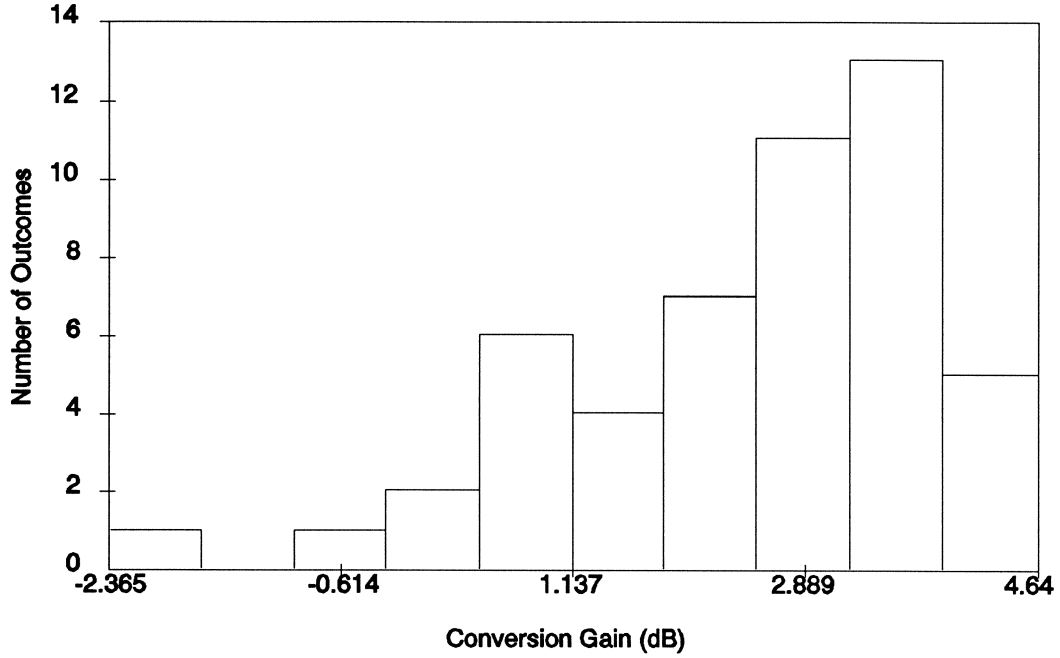
Fig. 20 Histogram of conversion gain at 7 GHz and 9 dBm input power. Couplings are not taken into account.

D. Circuit Optimization

In order to improve the responses of the doubler we use OSA90/hope to optimize the circuit. The specifications for optimization are

conversion gain > 3 dB
spectral purity > 20 dB

at 7 GHz and 9 dBm input power. The spectral purity is calculated by

$$\text{spectral purity} = P_2 / (P_1 + P_3 + P_4)$$

where P_i is the output power at the ith harmonic.

The optimization is performed based on the situation of Case III where both the coupling of the third harmonic stubs situated at the gate and drain ports of the FET and the effect of the bias pads are considered. A total of 15 variables are selected for optimization as indicated in Fig. 21.

Fig. 21 The doubler circuit and optimization variables.

Optimization Systems Associates Inc.

The minimax optimizer of OSA90/hope is used for this circuit optimization. All specifications are satisfied after optimization. The values of the variables before and after optimization are listed in Table I.

TABLE I
VARIABLE VALUES BEFORE AND AFTER OPTIMIZATION

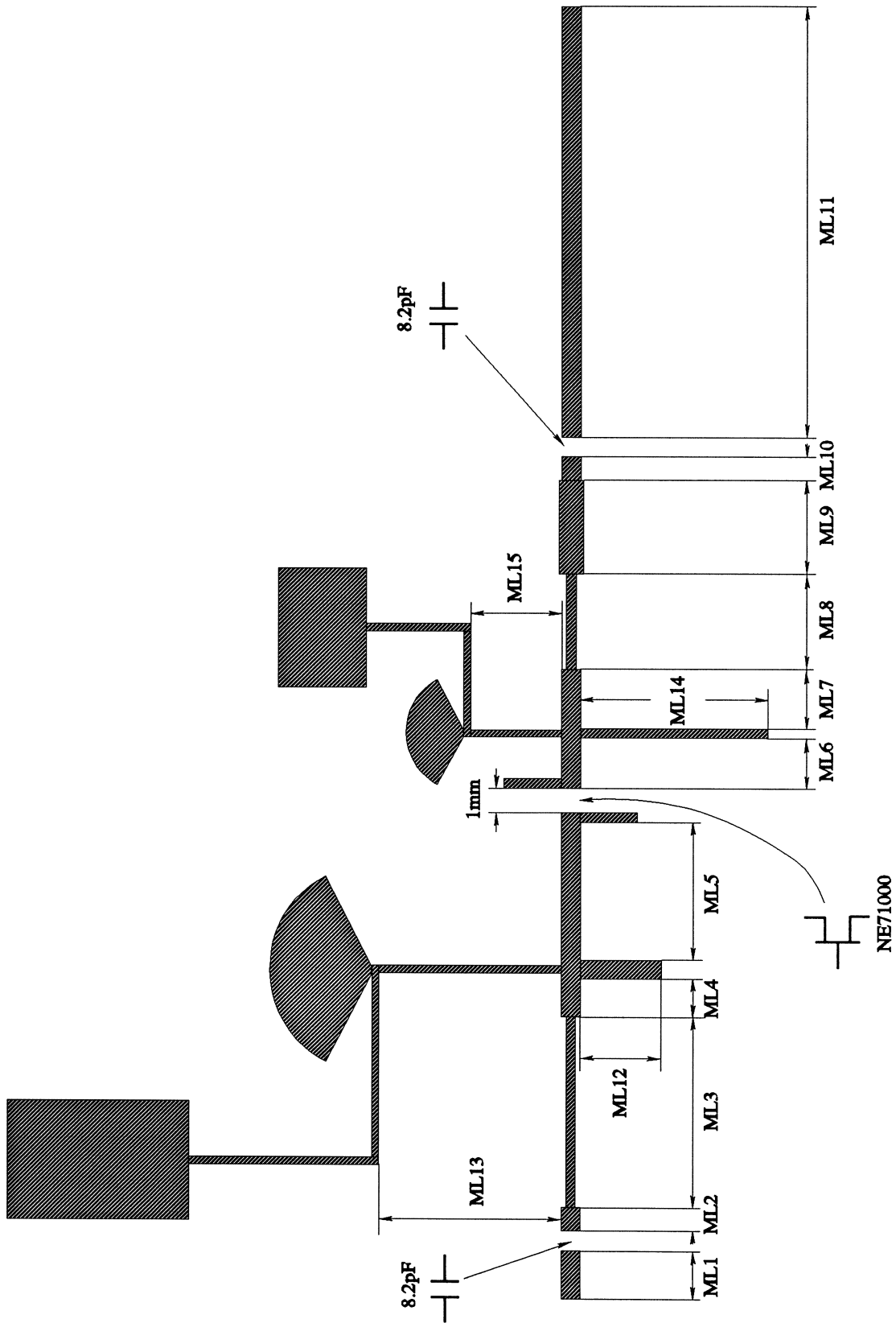| Variable	Before Optimization	After Optimization
ML1	2.0	1.691
ML2	1.0	0.901
ML3	7.95	6.792
ML4	1.55	1.759
ML5	5.75	5.182
ML6	2.11 + 0.38	1.601 + 0.38
ML7	2.5	2.842
ML8	3.99	3.903
ML9	3.87	3.698
ML10	1	0.994
ML11	20	17.35
ML12	3.395	4.500
ML13	7.68	7.510
ML14	7.85	7.903
ML15	3.82	3.804

All dimensions are in mm.

From Table I we can see that the most influencing variables are ML3, ML11 and ML12. The output power and conversion gain versus input power at 7 GHz are shown in Figs. 22 and 23, respectively. The output power and conversion gain versus frequency at 9 dBm input power are shown in Figs. 24 and 25, respectively. A 3D view of conversion gain versus frequency and input power is given in Fig. 26. The input and output voltage waveforms at 7 GHz and 9 dBm input power are plotted in Fig. 27.

Comparing Figs. 22-27 with Figs. 13-18 we can see that better circuit performance is achieved after circuit optimization.

Fig. 22   Output power versus input power at 7 GHz after optimization. The couplings between the third harmonic stubs and between the bias pads and the corresponding radial stubs are simulated by *em* [3].

Fig. 23   Conversion gain versus input power at 7 GHz after optimization. The couplings between the third harmonic stubs and between the bias pads and the corresponding radial stubs are simulated by *em* [3].

Output Power Spectrum Versus Frequency

Fig. 24 Output power versus frequency at 9 dBm input power after optimization. The couplings between the third harmonic stubs and between the bias pads and the corresponding radial stubs are simulated by *em* [3].

Fig. 25 Conversion gain versus frequency at 9 dBm input power after optimization. The couplings between the third harmonic stubs and between the bias pads and the corresponding radial stubs are simulated by *em* [3].

18

Fig. 26   3D view of conversion gain after optimization. The couplings between the third harmonic stubs and between the bias pads and the corresponding radial stubs are simulated by *em* [3].
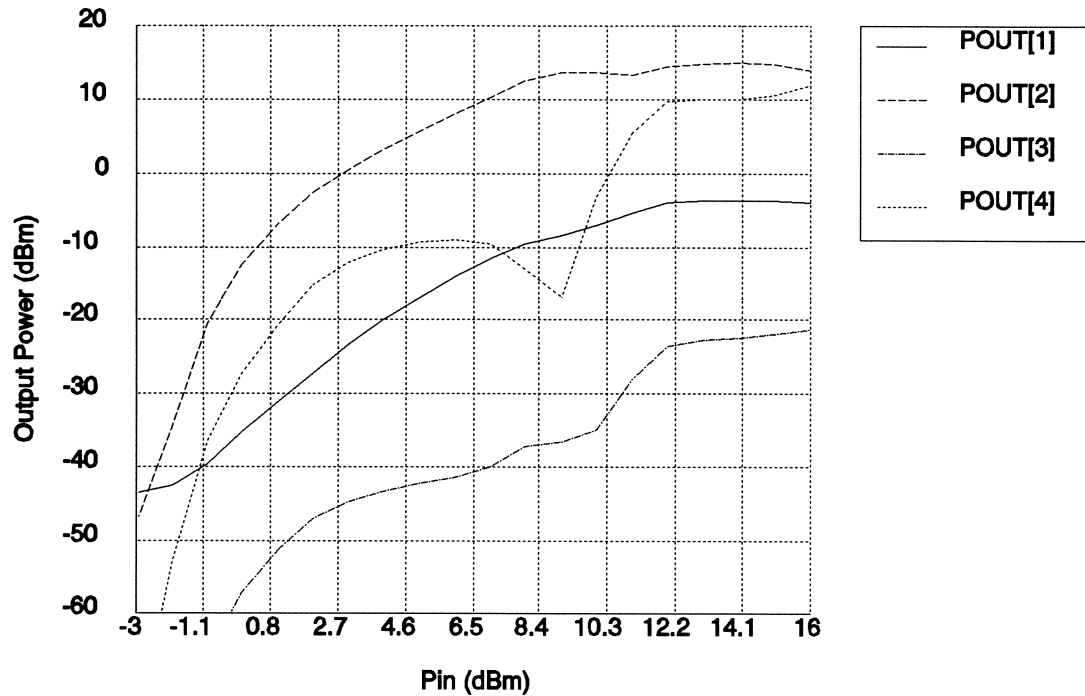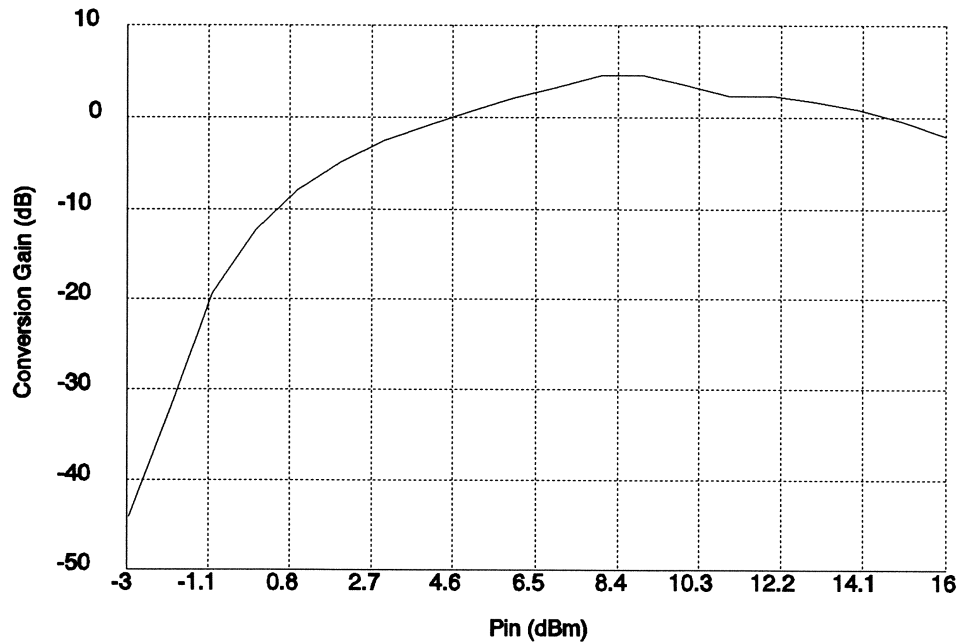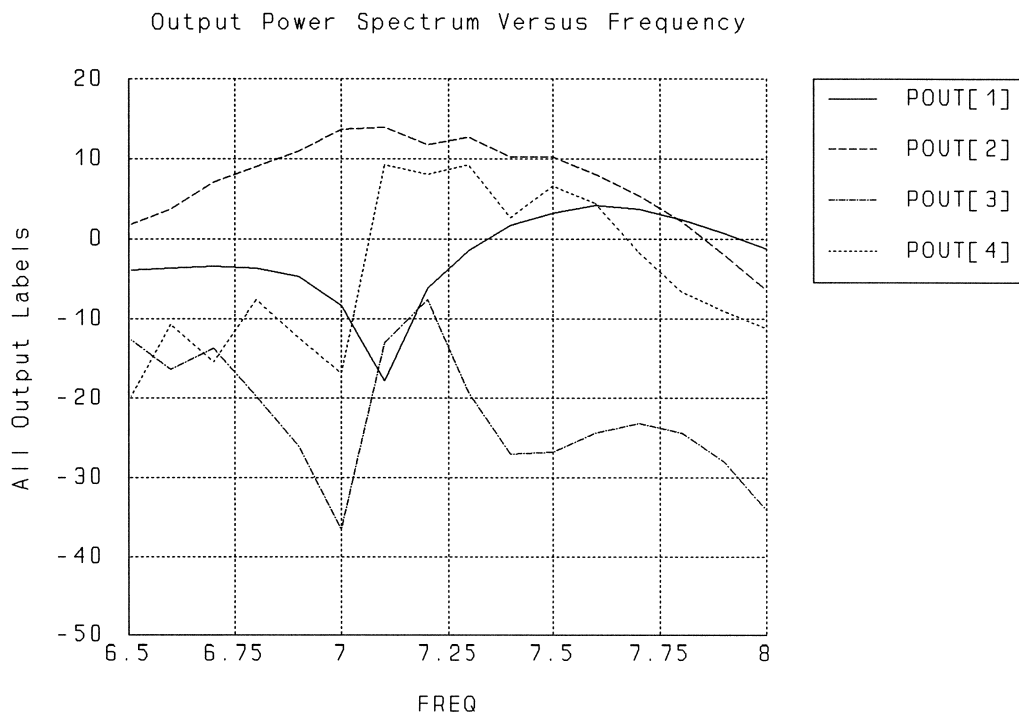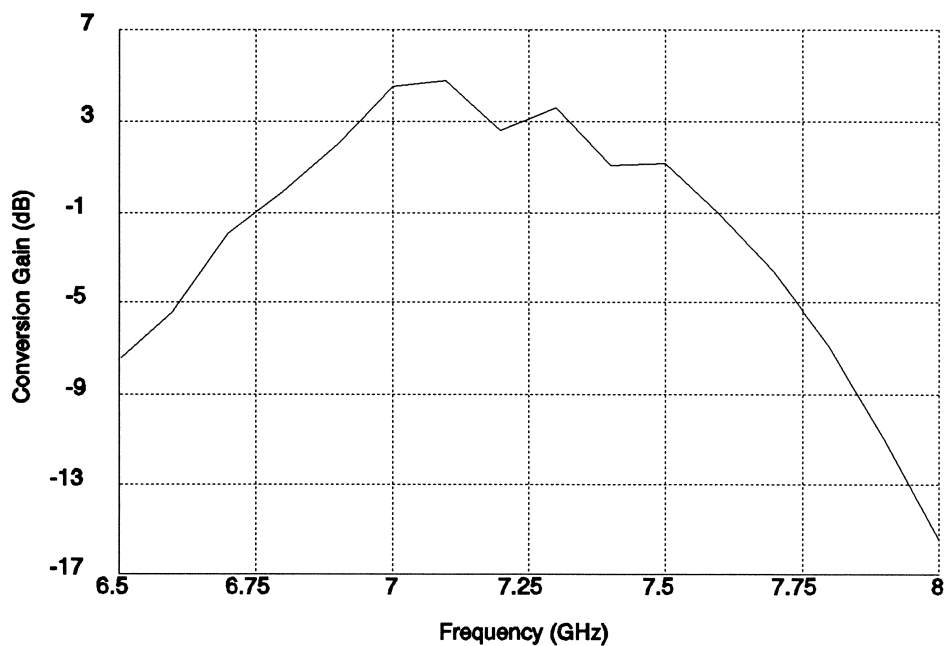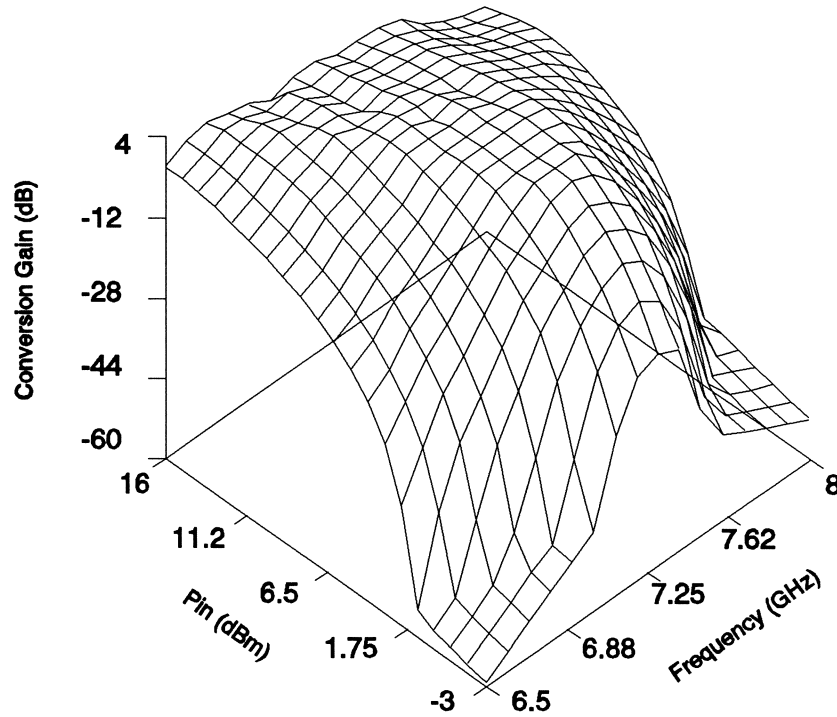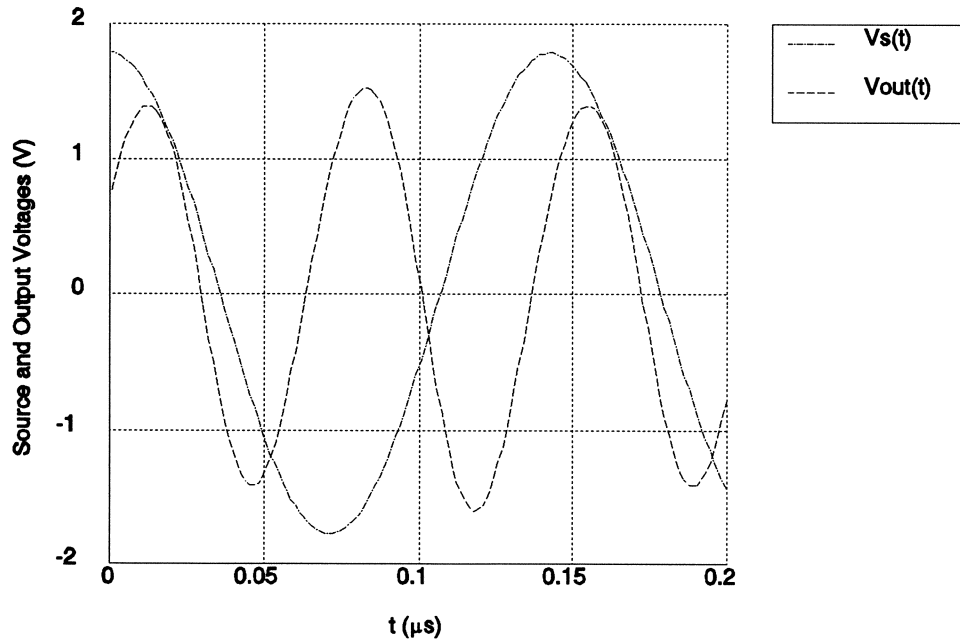

Fig. 27   Source and output voltages at 7 GHz and 9 dBm input power after optimization. The couplings between the third harmonic stubs and between the bias pads and the radial stubs are simulated by *em* [3].

19

Optimization Systems Associates Inc.

E. Simulation Time

All the experiments reported here were carried out on a Sun SPARCstation 10 workstation. The total time for simulating the complete circuit in Case I with the OSA90/hope built-in models for all the elements including the FET and distributed elements at 320 points (frequency: from 6.5 GHz to 8 GHz with 0.1 GHz step, input power: from -3 dBm to 16 dBm with 1 dBm step) is 1 minute and 45 seconds, about 0.3 second per point.

F. References

[1]   *HarPE™*, Optimization Systems Associates Inc., P.O. Box 8083, Dundas, Ontario, Canada L9H 5E7, 1993.

[2]   *OSA90/hope™*, Optimization Systems Associates Inc., P.O. Box 8083, Dundas, Ontario, Canada L9H 5E7, 1993.

[3]   *Em* Version 2.4, Sonnet Software, Inc., Suite 203, 135 Old Cove Road, Liverpool, NY 13090-3774, 1993.

[4]   "RF and Microwave Semiconductors," *NEC Data Book*, California Eastern Laboratories, 1994.

Appendix: The Circuit File for Case I

```
! dbl_c31.ckt
! Simulation of a Class B frequency doubler
! CAD benchmark example provided by Microwave Engineering Europe
! Model used: built-in Curtice and Ettenberg model extracted by HarPE
! The coupling between the 2 stubs at gate and drain and the effect
! of bias pads are not considered
! All the distributed elements are modelled by OSA90/hope's built-in models

Model
    MSUB   EPSR=2.2  H=0.254mm  T=0.0178mm  ROC=2.44e-8  RHS=0.001mm;

    MSL      1    2    W=0.76mm    L=2.0mm;
    CAP      2    3    C=8.2pf;
    MSL      3    4    W=0.76mm    L=1.0mm;
    MSTEP    4    5    W1=0.76mm   W2=0.4mm;
    MSL      5    6    W=0.4mm     L=7.95mm;
    MSTEP    6    7    W1=0.4mm    W2=0.76mm;
    MSL      7    8    W=0.76mm    L=1.55mm;
    MCROSS  10    8    9   11   W1=0.76mm  W2=0.76mm  W3=0.3mm;
    MSL     11   12    W=0.76mm    L=5.75mm;
    MTEE    12   13   14   W1=0.76mm  W2=0.38mm  W3=0.76mm;
    MTEE    15   16   17   W1=0.76mm  W2=0.38mm  W3=0.76mm;
    MSL     17   18    W=0.76mm    L=2.11mm;
    MCROSS  20   18   21   19   W1=0.38mm  W2=0.76mm  W3=0.3mm;
    MSL     19   22    W=0.76mm    L=2.5mm;
    MSTEP   22   23    W1=0.76mm   W2=0.38mm;
    MSL     23   24    W=0.38mm    L=3.99mm;
    MSTEP   24   25    W1=0.38mm   W2=1.04mm;
    MSL     25   26    W=1.04mm    L=3.87mm;
    MSTEP   26   27    W1=1.04mm   W2=0.76mm;
    MSL     27   28    W=0.76mm    L=1mm;
    CAP     28   29    C=8.2pf;
    MSL     29   30    W=0.76mm    L=20mm;
    MSL     10   31    W=0.76mm    L=3.395mm;
    OPEN    31;
    MSL     13   32    W=0.38mm    L=2.4mm;
    OPEN    32;
    MSL     16   42    W=0.38mm    L=2.4mm;
    OPEN    42;
    MSL     20   33    W=0.38mm    L=7.85mm;
    OPEN    33;
    MSL      9   34    W=0.3mm     L=7.68mm;
    MTEE    34   35   36   W1=0.3mm  W2=0.3mm  W3=0.3mm;
    MSL     36   37    W=0.3mm     L=7.68mm;
    MBEND2  37   38    W=0.3mm;
    MSL     38   39    W=0.3mm     L=7.68mm;
    MSTEP   39   40    W1=0.3mm    W2=5.0mm;
    MSL     40   41    W=5.0mm     L=7.42mm;
    MSL     21   43    W=0.38mm    L=3.82mm;
    MTEE    43   44   45   W1=0.3mm  W2=0.3mm  W3=0.3mm;
    MSL     45   46    W=0.3mm     L=4.1mm;
    MBEND2  46   47    W=0.3mm;
    MSL     47   48    W=0.3mm     L=4.1mm;
    MSTEP   48   49    W1=0.3mm    W2=5.0mm;
    MSL     49   50    W=5.0mm     L=3.7mm;
    MRSTUB  35    W=0.3mm   L=4.45mm   ANG=130;
    MRSTUB  44    W=0.3mm   L=2.3mm    ANG=130;

    EXTRINSIC4   141  142  143  14  15
        RG=1.33301          RD=0.888452        RS=5.04386
        CDS=0.0414509pF  GDS=0.00441929   CX=100pF
        LG=0.160598nH    LD=5.3121e-06nH  LS=0.0718402nH
        CGE=0.143109pF   CDE=0.0924559pF;

    FETC 141 142 143
        A0=0.0826627    A1=0.335942    A2=0.367757    A3=0.00858573
        GAMMA=1.86239   BETA=0.121412  VDS0=0.742967  IS=5.26136e-11
        N=3.28559       CGD0=0.108206pF CGS0=0.227312pF FC=0.173912e-12
```

```
        Tau=1.0947ps   Gmin= 0.841032e-12;

VGS=-1.2;
VDS=3;
IND      41    411 L=1000nH;
IND      50    501 L=1000nH;
VSOURCE 411  0    NAME=B_VGS  VDC=VGS;
VSOURCE 501  0    NAME=B_VDS  VDC=VDS;

PIN = 9dBm;
PORT.in  1  0  P[1]=PIN  R=50;
PORT     30 0  NAME=OUT  R=50;

CIRCUIT;

Pout[0:N_SPECTRA] = if (PWout > 0) (10 * log10(PWout) + 30) else (NAN);

Vs: sqrt(400 * 10^((Pin - 30)/10));
MVs[0:N_SPECTRA] = [0 Vs 0 0 0];
PVs[0:N_SPECTRA] = 0;

Conversion_Gain = POUT[2] - PIN;
End

Sweep
   HB: FREQ: 7GHZ Pin: from -3dBm to 16dBm step=1dBm
       Pout Conversion_Gain MVout PVout MVs PVs
       {Xsweep title="Output Power Versus Input Power at 7GHz"
        Y=Pout[1].green & Pout[2].red & Pout[3].yellow & Pout[4].pink
        NXticks=10  Ymin=-60 Ymax=20 NYticks=8}
       {Xsweep title="Conversion Gain Versus Input Power at 7GHz"
        Y=Conversion_gain.green NXticks=10 Ymin=-50 Ymax=10 NYticks=6}
       {Waveform  Title="Frequency Doubler Source and Output Voltage Waveforms"
        Spectrum=(MVs, PVs)."Vs(t)" & (MVout, PVout)."Vout(t)"
        Tmin=0 Tmax=0.2 NT=150  Ymin=-2 Ymax=2 NYTicks=4 pin=9};

   HB: FREQ: from 6.5GHZ to 8GHZ step 0.1GHZ
       Pin: from -3dBm to 16dBm step=1dBm
       Pout Conversion_Gain
       {Xsweep title="Output Power Versus Frequency at 9 dBm Input Power"
        Y=Pout[1].green & Pout[2].red & Pout[3].yellow & Pout[4].pink
        NXticks=6  Ymin=-50 Ymax=20 NYticks=7 Pin=9}
       {Xsweep title="Conversion Gain Versus Frequency at 9 dBm Input Power"
        Y=Conversion_Gain.green NXticks=6  Ymin=-17 Ymax=7 NYticks=6 Pin=9}
       {Visual Z=Conversion_Gain Z_title="CG" Zmin=-60 Zmax=4 Lines=ON
        Frame=OFF Paint=OFF Smooth=ON}
End
```